On the investigation of the most critical shape imperfections for wind turbine tower shell structures

Kshitij Kumar Yadav[1], Jens Lycke Wind[2], Simos Gerasimidis[3]

Abstract
As the wind power industry is the fastest growing energy resource in the world, wind turbine structures have been continuously increasing their dimensions and in particular their height, a trend which is expected to continue in the future. The height of wind turbines has doubled during the last 10 years and their power has increased by a factor of 5. This increase in height comes along with an overwhelming increase in the construction cost as well as with a plethora of emerging problems involving design/construction/erection processes. The present paper studies the problem of the most critical geometrical imperfections for the buckling capacity of wind turbine tower shell structures. The presented study is applied to many different tower geometries and includes linear elastic as well as plastic buckling through a series of nonlinear finite element calculations. The most critical geometrical shape imperfection is calculated through the parametric interaction of the buckling modes of the shell tower structure. The results present the sensitivity of the buckling capacity of the shell structure to the interaction of the modes considered as the geometrical onset for the nonlinear finite element analysis. The produced interactions are compared to the widely applied Eurocode design codes and useful conclusions are drawn.

1. Introduction

The use of wind turbines is increasing continuously and it is anticipated that this trend will accelerate in the coming future. The need for more vigorous wind harvesting has given impetus to many technological advances, but also to making more efficient and less expensive wind turbines. Among the many technical goals of today's wind energy industry is to develop solutions for taller wind turbine towers. The increase in height of wind turbine towers is imperative to achieve these goals as the wind profile is stronger at higher heights (Khatri 2010). However, making higher wind turbine tower structures, poses numerous challenges to structural engineers.

Traditionally, thin hollow cylindrical shells are used for making wind turbine towers due to their economical and constructional advantages. It is well known from the groundbreaking work by

---

[1] PhD Candidate, University of Massachusetts, Amherst, <kkyadav@umass.edu>
[2] Structural Engineer, Vestas Wind Systems A/S, <jelcw@vestas.com>
[3] Assistant Professor, University of Massachusetts, Amherst, <sgerasimidis@umass.edu>

Koiter (1945) that cylindrical shells are highly imperfection sensitive structures when subjected to compressive stresses. This property of course depends on their characteristics and mainly on how thin they are in terms of R/t (R is the radius and t the thickness of the shell). In addition, their capacity depends strongly on the extent of residual stresses due to manufacturing or construction and assembly process. For wind turbine towers, the increase in height renders the stability and imperfection sensitivity of the tower as very important design issues.

Wind turbine tower structures are mainly subjected to bending moment coming from the lateral wind load and axial force coming from the weight of the nacelle placed at the top the tower. The study of cylindrical shells (not necessarily wind turbine structures) has occupied the research community for years (Hutchinson 1965, Kyriakides 1982, Karamanos 1991). However, the problem of the scale of very tall wind turbine towers is relatively new (Guo et. al. 2013, Abdulla et. al. 2015, Jay et. al. 2016).

This paper deals with the imperfection sensitivity of a real wind turbine tower under bending moment and studies the problem of worst shape geometric imperfection. The worst shape imperfection is defined as the shape of imperfection that leads to the lowest critical load of the structure (Lindgaard et. al. 2010, Deml et. al. 1997). For the present study, mode shapes of elastic buckling are taken as the pattern of geometric imperfection and their effect on the load carrying capacity is studied. The mechanism of buckling and the imperfection sensitivity of the tower are discussed in detail. Finally, the effect of variation of the amplitude of the imposed imperfection is also studied for the case which leads to the lowest critical load (the worst shape imperfection).

2. Geometry of the Tower and Finite Element Modeling
2.1 Mechanical Model
The geometry of the wind turbine tower for this study is a 3.6 MW Vestas turbine. The bottom of the tower is assumed to be fixed and the top of tower is assumed to be free. These assumptions are reasonable as the bottom of the tower is attached to the foundation and the top is attached to the rotor.

2.2 Finite Element Modeling
The simulation of this tower is done in the finite element package ABAQUS (2016). A total of 70195 S4R shell elements are used for the modeling. For simulating the boundary conditions and applied bending moment, two reference points have been created at the center of the top (RP-2) and the bottom ends (RP-1) of the tower (Fig. 1a). The edge shell nodes of the top and the bottom are attached to the reference points to form a rigid body constraint. Bending moment M_x is applied at RP-2, positively in the X direction.

Before an actual analysis of the tower can be performed, a mesh convergence study has been followed. It is found that the analysis converges when the number of elements is more than 50000 (using a uniform mesh). Abdulla et. al. (2015) have recommended that the size of mesh needs to be less than $0.5\sqrt{rt}$. The mesh size of the upper part of the tower is defined meeting this constraint and the lower part of tower is meshed with a less dense pattern (Fig. 1b, c and d). In between these zones, a mesh transition zone has been created to ensure the smooth transition of the lower and the upper part. This 2-zone distinction is applied since it was expected by the authors that instability phenomena would appear closer to the top of tower where the R/t values are lower. Thus the

density of mesh is higher at the top part than the bottom part as shown in Fig. 1c. This is done to save in computational time without any loss of numerical accuracy.
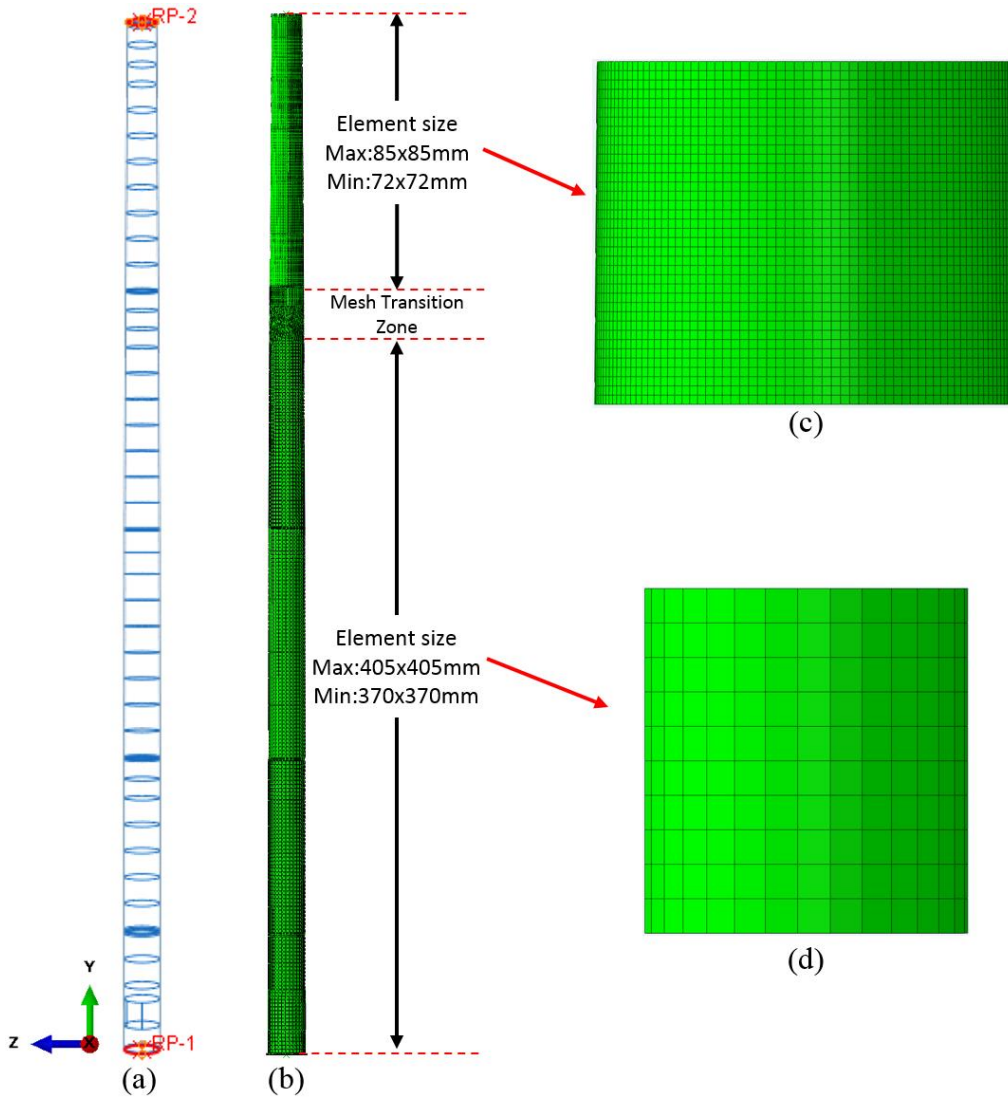

Figure 1: (a) Schematic diagram of wind turbine tower along with reference points RP-1 and RP-2, (b) tower with mesh elements and (c) the mesh density at the top and (d) the bottom part.

3. Results of the analysis
3.1 Nonlinear Static Analysis of Perfect Tower
First, the perfect tower is analyzed under the application of bending moment in ABAQUS to find out the critical moment and the mode of buckling. A force-controlled nonlinear static analysis procedure is applied for the analysis which incorporates geometric and material nonlinearities.

The deformed shape of the tower under the applied bending moment is shown in Fig. 2a and Fig. 2b, along with the longitudinal stresses S22. Fig. 2c presents a close-up view of the part of the tower which experiences the highest compressive longitudinal stresses S22. The directions of the

stresses used in this paper for the presentation of the results is provided in Fig. 2d. S22 represents the longitudinal stress, while S11 represents the hoop stress of the elements.

The detailed results at the nodes and elements of interest are included in Fig. 3. These elements and nodes are situated at the compressive side of flexure, as shown in Fig. 2(d) and thus the axial stress component S22 is always in compression. For the present simulation, 5 section integration points along the thickness of the S4R element have been chosen, defined as SP-1, SP-2, SP-3, SP-4 and SP-5, as seen in Fig. 2(d). S22 at SP-1 is always slightly more than at SP-5 as it is on the outer side of the cylinder, due to a bending moment within the thickness of the shell.
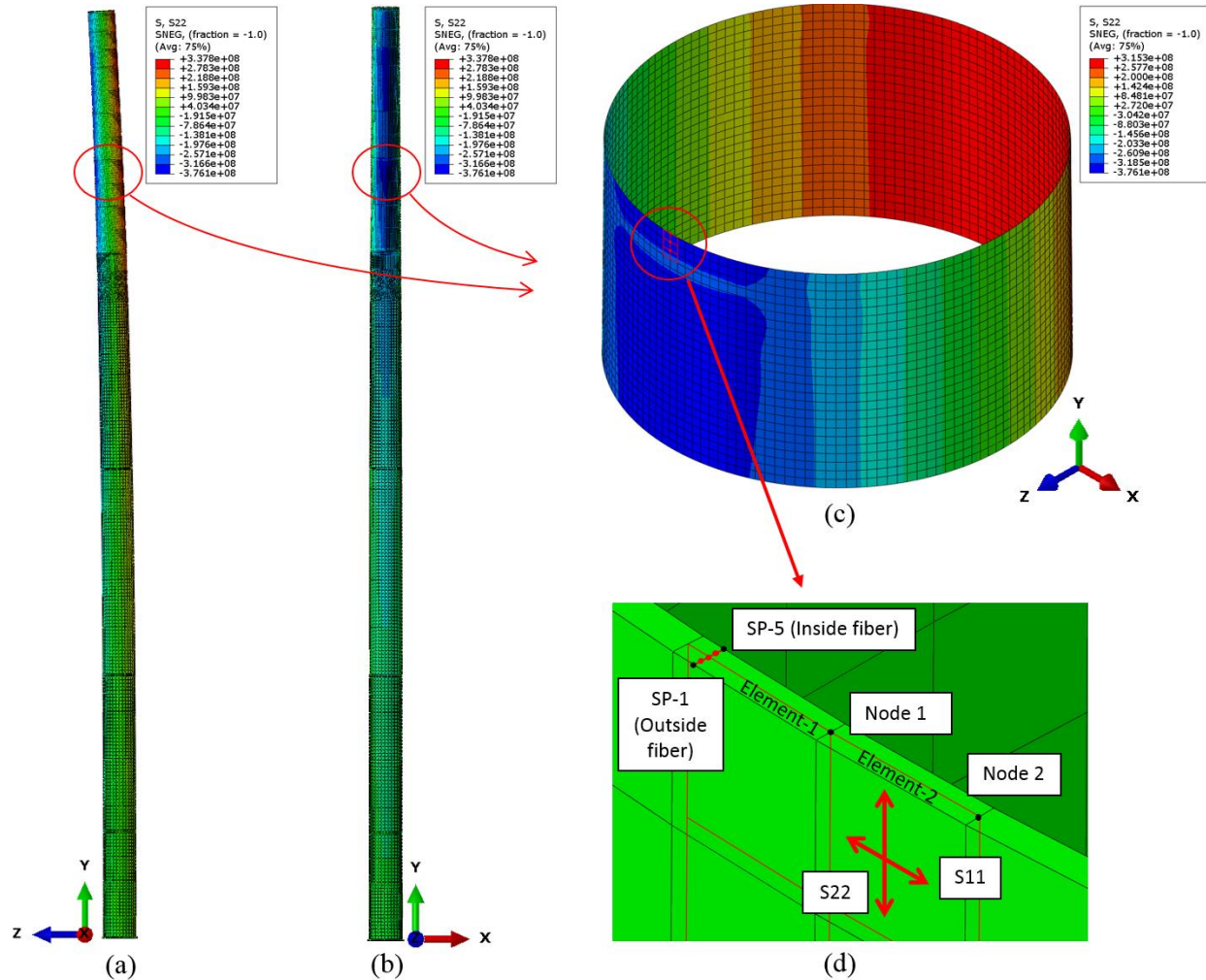

Figure 2: (a) Deformed shape of the tower in Y-Z plane, (b) deformed shape of the tower in X-Y plane, (c) location of Node-1, Node-2, Element-1 and Element-2 and (d) the direction of S22 and S11 along with location of SP-1 and SP-5.

Fig. 3a includes the compressive longitudinal stresses S22 of SP-1 and SP-5 at the integration point of Element-1. At the onset of the analysis, these stresses are varying linearly with M_x but after a certain value of M_x, abrupt changes take place and finally the analysis stops due to negative eigenvalues (static general is applied). It is worth mentioning that one fiber of the shell enters the hardening zone. As expected, this is SP-1 which belongs to the outer fiber of the element. The internal fiber of the shell, presented by SP-5 exhibits a stress relaxation. This behavior provides a

4

clear sign of instability and M_x at the end of analysis can be taken as the critical moment of the perfect tower. This moment will be referred to as $M_{perfect}$ in this study. It should also be noted that as the stresses have crossed the yield limit, the buckling is inelastic in nature.

Fig. 3b depicts the hoop stresses at the same element, again for two section points, SP-1 and SP-5, of the integration point of Element-1. Abrupt changes in the stress S11 close to the end of the analysis indicate the appearance of instability similarly to S22. In this case however, as expected, the stresses are well below the yielding point. This phenomenon is similar to the one described by Hutchinson (2010).
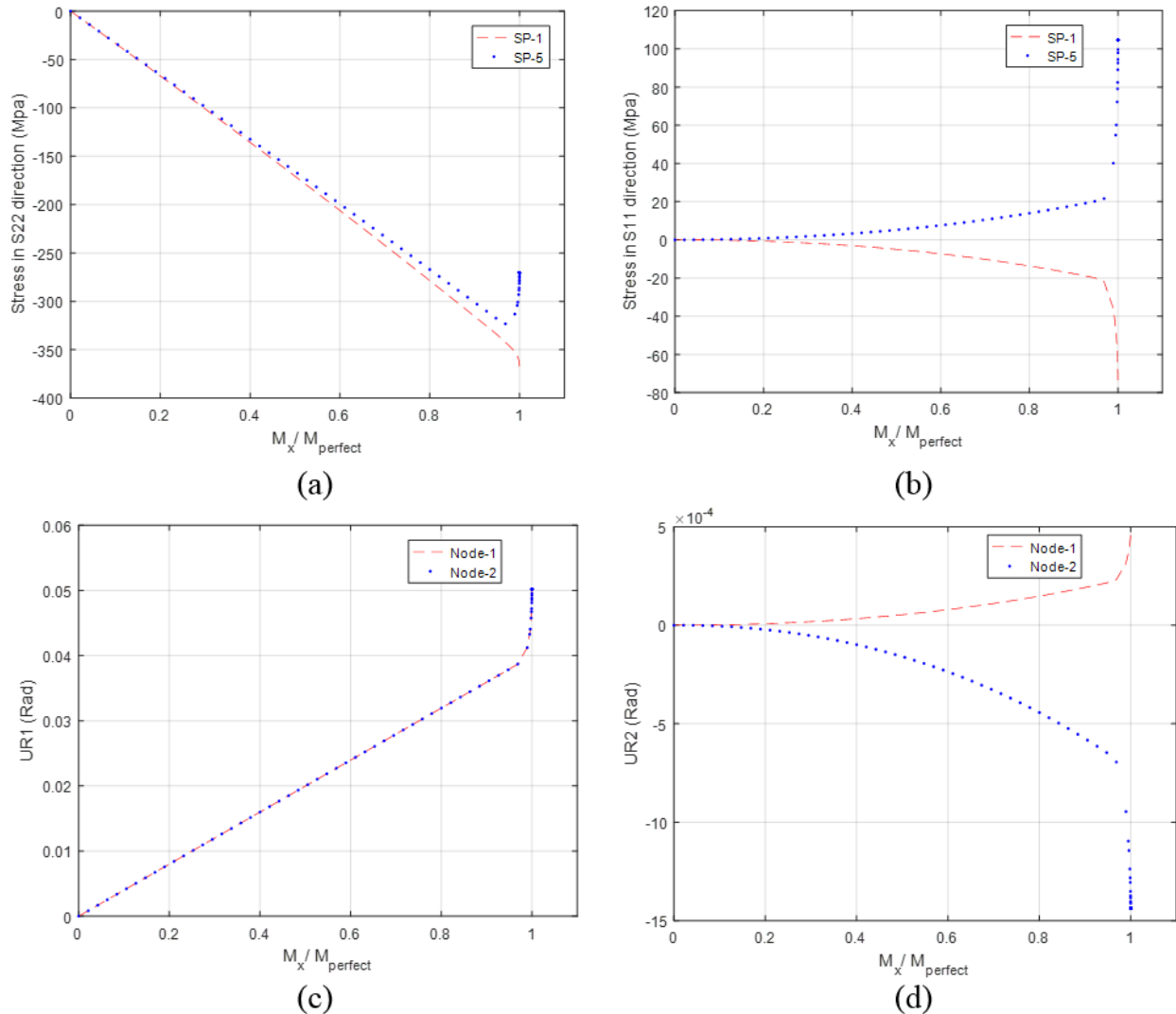

Figure 3: (a, b) Stresses at the integration point of element-1 and (c, d) the rotations at node-1 and node-2.

Buckling becomes more clear by the rotation at Node-1 (maximum stress node) and it neighboring Node-2 as shown in Fig. 3c and Fig. 3d, respectively. Initially, rotation around the X direction (UR1) at Node-1 and Node-2 increases linearly with applied moment M_x, but at the end rapid changes takes place, which is a strong indication of a shell instability condition (Fig. 3c). It must be mentioned at this point that these rotations refer to the end nodes of the shell and not to the shell

integration points. Rotation around the Y direction (UR2) as shown in Fig. 3d also indicates an instability condition close to the end of the analysis. UR2 at Node-1 and at Node-2 are in reverse directions which implies an instability is taking place as this becomes suddenly close to the end of the analysis.

It must be mentioned here that the location of the origin of the global coordinate systems results in un-symmetric UR2 (rotation around the global Y axis) between Node-1 and Node-2. As shown in Fig. 4, the origin of the x axis crosses Element-2 at a point which has a distance of 1/3 of the element width from one of its edges. If the axis would be crossing in the middle of the element, the UR2 rotation of Node-1 and Node-2 would be equal but opposite in signs.
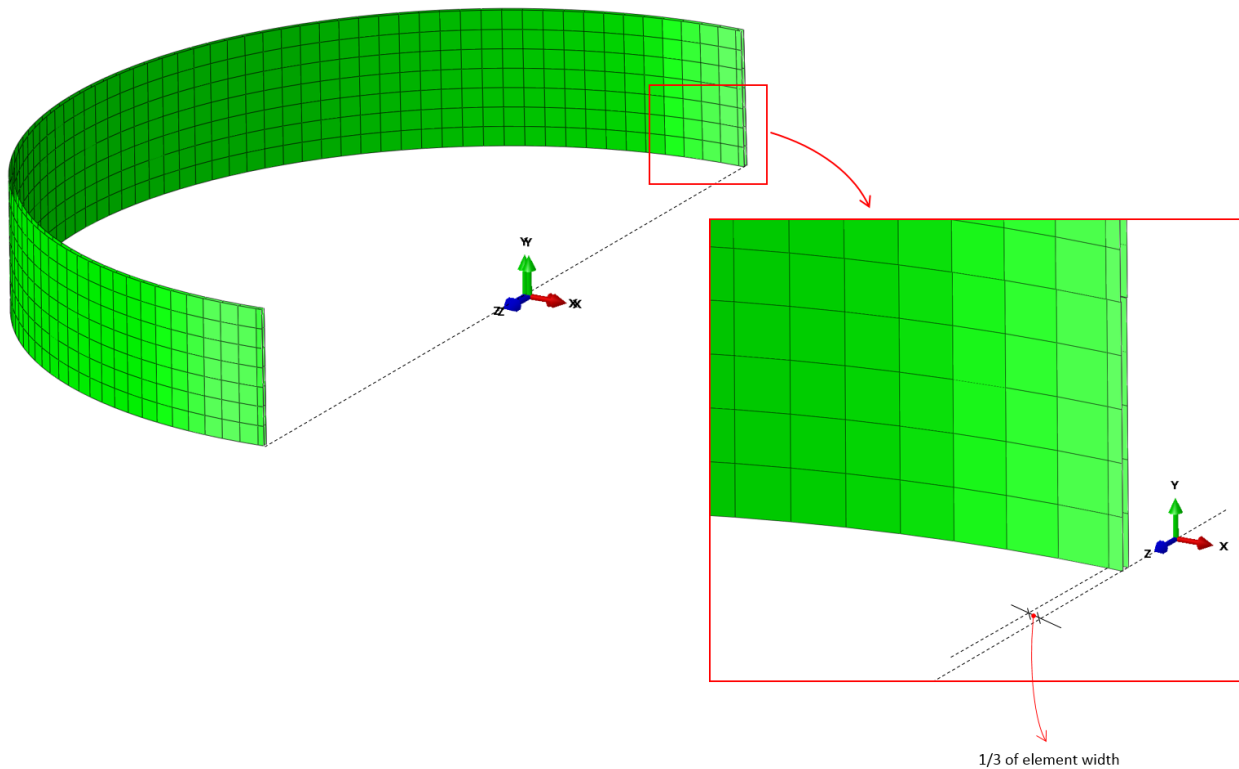

Figure 4: Mesh and origin of axes.

3.2 Elastic Buckling Analysis of Perfect Tower
To introduce the geometric imperfections, the mode shapes of elastic buckling are utilized. Eigenvalue analysis is performed using the linear perturbation method on the tower to get the eigenvalues and mode shapes. The result of eigenvalue analysis is shown in Fig. 5 which includes the eigenvalues of the first 100 modes. It can be seen that the first 100 eigenvalues are very close to each other which is an expected behavior of thin cylindrical shells. Indicatively, the first 20 modes are within 12% of the first eigenvalue, the first 50 are within 22% of the first eigenvalue and the first 100 eigenvalues lie between 30% of the first eigenvalue.

The shape of the eigenmodes is of great interest. The first modes include a longitudinal wrinkling buckle-wave. As the mode number increases, the mode becomes more a combination of longitudinal along with circumferential buckle-waves. For these first modes, buckling takes place at the location where the R/t ratio is minimum (the shell is the "thinnest"), which is also an

expected behavior of cylindrical shells (NASA, 1965). In Fig.6c, the shape of the first six eigenmodes is shown.
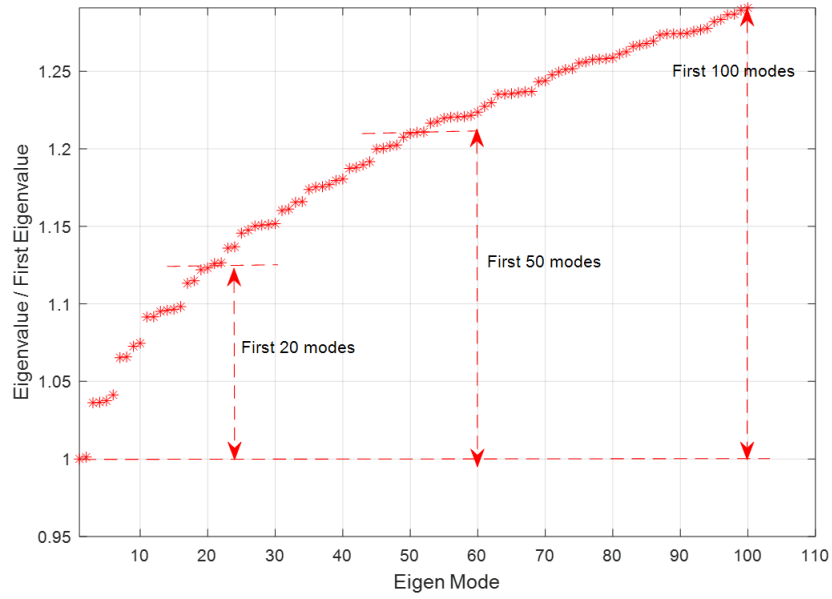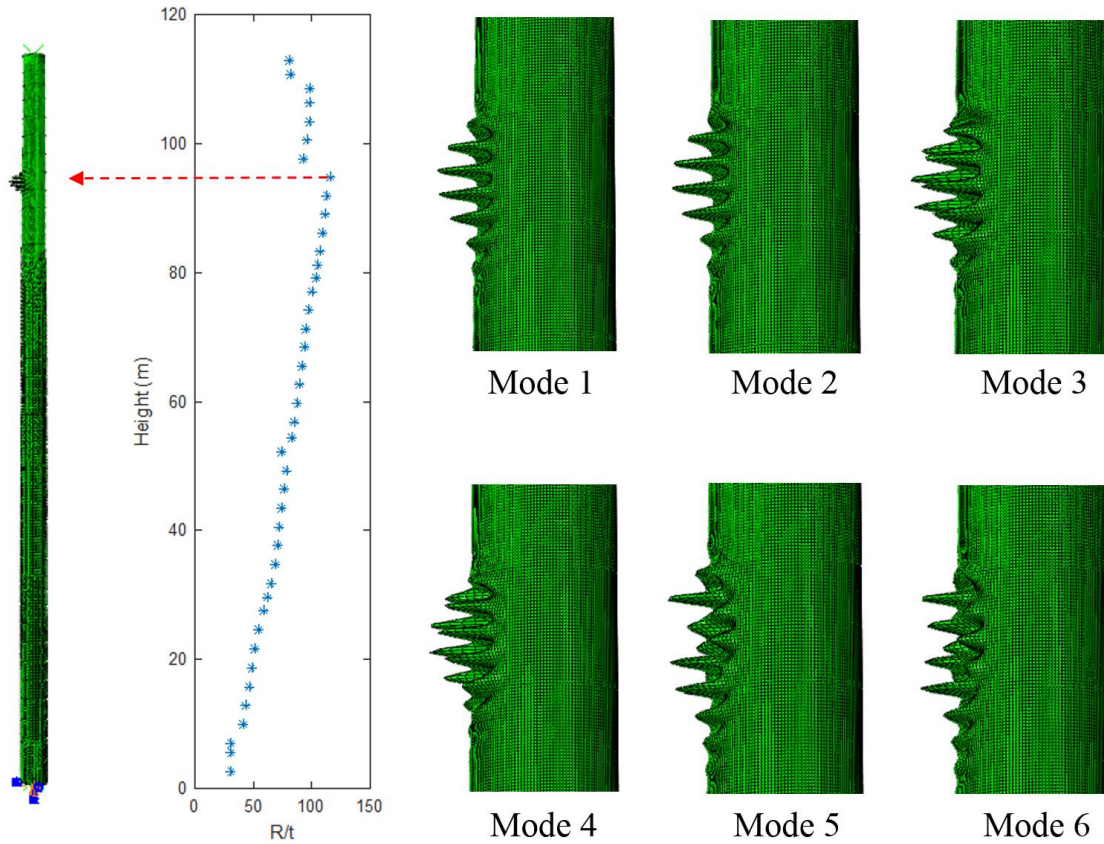

Figure 5: Variation of eigenvalues with eigenmodes

Figure 6: (a) First eigenmode of the tower, (b) variation of R/t along the height and (c) detailed view of the first six eigemodes.

3.3 Nonlinear Static Analysis of the geometrically Imperfect Tower

To study the effect of geometric imperfections on the tower, imperfections are introduced in the form of eigenmodes. First, the effect of imperfections in the form of individual modes has been studied. Then, the effect of modes interaction has been studied, combining the first three and then the first five modes. Combinations of more than five modes was not done due to the extensive computational time required. For this particular study of this section, the amplitude of geometric imperfections is taken as $t/10$ (t is the thickness of the shell at the location of the buckle-waves).

3.3.1 Geometric Imperfections in the Shape of Individual Modes

Geometric imperfections in the form of the first 50 mode shapes are introduced in the perfect tower using ABAQUS command IMPERFCTION. Mode shapes are scaled such that the amplitude of the imperfection is $t/10$. After the imperfections have been introduced, a nonlinear static analysis is performed on the 50 imperfect towers.

In all cases, inelastic buckling takes place as in the case of the perfect tower and the deformed shape is similar to the one of the perfect tower. The critical bending moment of each imperfect tower is shown in Fig. 7 in the form of the ratio λ which is the critical moment of the imperfect tower over the critical moment of the perfect tower. It can be seen that the imperfection reduces the moment carrying capacity of the tower. However, this reduction is relatively small compared to the knock-down factors by Hutchinson (2010), which of course include all possible decreasing effects. A first conclusion which can be derived from this analysis is that this particular tower is not very imperfection sensitive for bending moment. This can also be attributed to the inelastic buckling mode; inelastic buckling is not as sensitive to imperfection as elastic buckling (Wunderlich 2000). In any case, the mode shape which has the biggest effect on the capacity of the tower is Mode-2, decreasing the capacity by 6 %($\lambda = 0.94$).

In Fig. 7, there are eignemode-based imperfections which lead to critical moments which are higher than the critical moment of the perfect tower (λ>1). These values can be attributed potentially to buckle-waves that may require a denser mesh than the one used in this model. However, since they appear for modes higher than the 20th one, it was not considered as high priority for further study at this point.
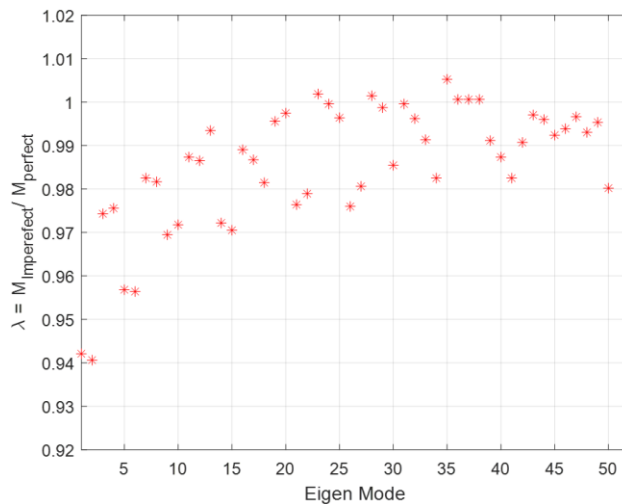

Figure 7: Effect of imperfections on the critical bending moment (individual modes)

3.3.2 Imperfection in the Shape of the First Three Modes Interaction
The effect of imperfections in the shape of combinations of the first three modes has also been studied. The geometric imperfections in this case are defined by the following rule:

$$\phi = (\frac{t}{10})\sum_{i=1}^{3} a_i \phi_i \tag{1}$$

In this equation, ϕ is the imperfection vector expressed by nodal coordinates, ϕ_i is the normalized i^{th} mode and a_i is the contribution of ith mode which is chosen such that:

$$\sum_{i=1}^{3} a_i = 1,$$
$$a_i \in \{0, 0.25, 0.50, 0.75, 1\} \tag{2}$$

This constraint makes sure that the amplitude of the imperfection shape is always $t/10$. Although infinite combinations are possible to satisfy this constraint if a continuous computation is selected, due to the extensive computational time required, only five discrete values of a_i are considered in this study as shown in Eq. (2).

From these two constraints on a_i, a total of 15 different expressions for geometric imperfections are generated using the first three modes. All these 15 shapes are introduced individually in-turn and a nonlinear static analysis is performed. The results are shown in Table 1 arranged in increasing order of ratio λ. It can be seen that the combination which contains only the second mode leads again to the minimum value of critical the bending moment.

The unstable equilibrium is again found to be an inelastic buckling mode.

Table 1: Critical Bending Moment for interaction of the First 3 Modes

a_1	a_2	a_3	$\lambda = \dfrac{M_{imperfect}}{M_{perfect}}$
0	1.00	0	0.940632
1.00	0	0	0.942105
0.25	0.75	0	0.956421
0	0.75	0.25	0.957053
0.75	0.25	0	0.957684
0.75	0	0.25	0.961053
0.50	0.50	0	0.963789
0	0.50	0.50	0.969263
0.25	0.50	0.25	0.971368
0.50	0.25	0.25	0.973474
0.50	0	0.50	0.973474
0	0.25	0.75	0.974316
0	0	1.00	0.974526
0.25	0.25	.50	0.9800
0.25	0	.75	0.980632

3.3.3 Imperfection in the Shape of the First Five Modes Interaction

The first five modes are also combined to look further for a worse geometric imperfection. The formulation for the interaction is similar to the three mode combination, except that five modes are used now instead of three. The imperfection ϕ in this case is defined as:

$$\phi = (\frac{t}{10})\sum_{i=1}^{5} a_i \phi_i \tag{3}$$

$$\sum_{i=1}^{5} a_i = 1, \tag{4}$$
$$a_i \in \{0,0.25,0.50,0.75,1\}$$

A total of 70 different shape imperfections have been generated and nonlinear static analysis is performed. It is found that for this case imperfection Mode-2 leads again to the minimum critical moment. From these studies, imperfection in the shape of Mode-2 seems to be the worst shape imperfection for this specific tower geometry.

3.3.4 Mechanism of Collapse of Mode 2 Shape Imperfect Tower

Detailed analysis of the results around the region which contains the nodes with maximum stresses has been done for the case of the imperfect tower as well.

Stresses at the integration point of Element-1 are shown in Fig. 8a and in Fig. 8b. Fig. 8a includes the longitudinal stresses S22 of SP-1 and SP-2 at the integration point of Element-1. This element is located at the compressive side of flexure and thus the axial component S22 is always in compression. Initially, S22 is varying linearly with M_x but after a certain value of M_x abrupt changes take place and finally analysis stops at $M_x = 0.9406 M_{perfect}$ due to negative eigenvalues (again static general is applied). Abrupt changes in S11 are also taking place demonstrating the same instability mode (Fig. 8b). These are the clear sign of instability and M_x at the end of analysis can be taken as the critical bending moment.
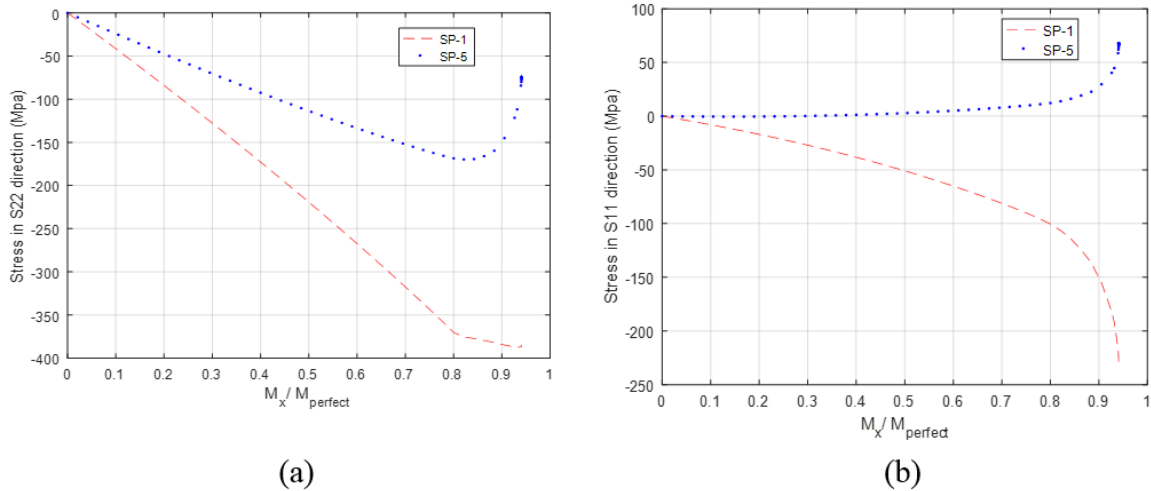

(a)   (b)

Figure 8: (a) Stress S22 at SP-1 and SP-5 at the integration point of Element-1 and (b) S11 stresses at the same points

10

Instability becomes more visible by the rotation of Node-1 and Node-2. Rotation around the X direction (UR1) is shown in Fig. 9a and two important observations can be made from this plot. The first observation is that UR1 is almost the same for Node-1 and Node-2 and the second observation is that at the end of the analysis there is a reversal behavior. These observations indicate the instability condition of the tower at the end. Rotation around the Y direction (UR2) is shown in Fig. 9b. UR2 at Node-1 and Node-2 are in opposite directions for the reason described in section 3.1. Again, the final part of these graphs implies an instability is taking place as this becomes sudden close to the end of analysis.
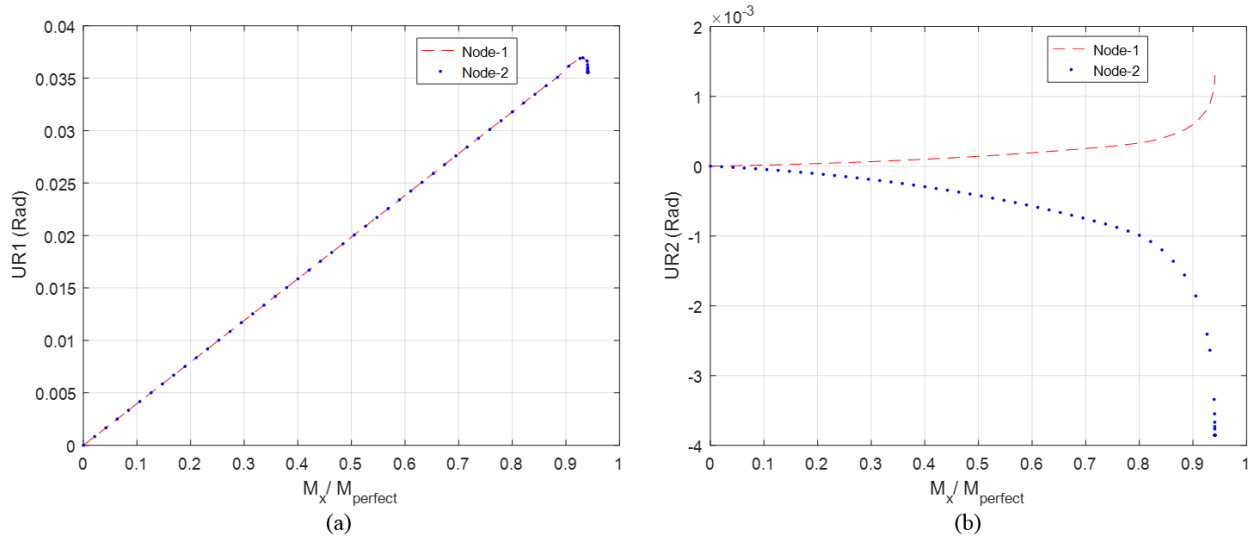

Figure 9: (a) Rotation in the global X direction at Nodes-1 and 2 and (b) rotation in Y direction at the same nodes.

3.3.4 Effect of the Amplitude on Mode 2 Shape Imperfect Tower

The effect of the amplitude of imperfection on the reduction of the critical moment has also been studied. Only one mode was chosen for this study and this was mode 2 as it was shown to be the most critical imperfection shape among the 135 cases studied. The results are shown in Fig. 10.
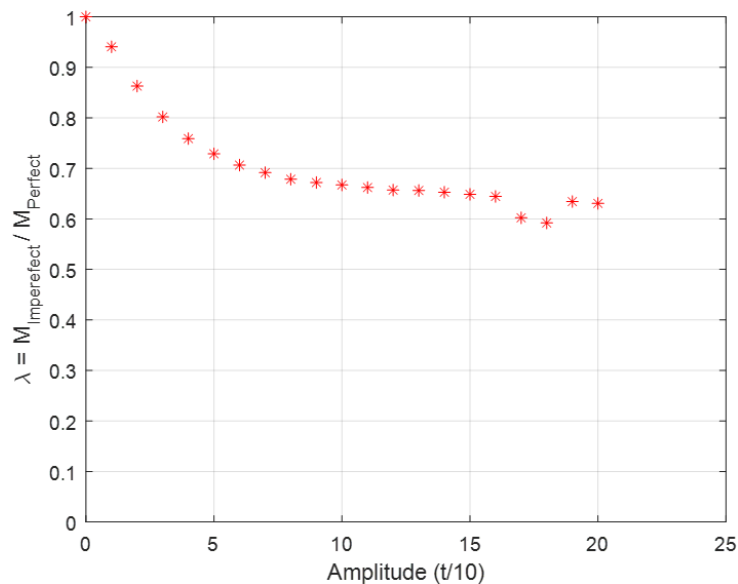

Figure 10: Effect of Mode-2 imperfection amplitude on critical moment

11

Generally, the increase in the amplitude of imperfection increases the reduction in the critical moment. For small values of amplitude, the reduction is rapid but for amplitude more than $6 \times (\frac{t}{10})$, the reduction becomes very slow. It can be said that as the structure becomes more and more imperfect its sensitivity stabilizes. Similar observations were found by Schneider et. al. (2004).

4. Conclusions

This study investigated worst shape geometric imperfections on the application of bending moment for a particular steel cylindrical shell wind turbine tower. Mode shapes of elastic bucking analysis are used for the shape of imperfections. Individual mode shapes and the combination of the first three and the first five mode shapes are introduced in the tower as imperfections. Static nonlinear analysis is applied to find out the reduction in the critical moment due to the imperfection and it is found that the imperfection in the form of mode 2 provides the worst shape imperfection. Apart from that, it is also observed that the tower is not very sensitive to geometric imperfections for the bending moment and inelastic local bucking takes place in all analysis.

This analysis is limited in many respects; i.e., shape of imperfection is created by mode shapes, only geometric imperfections are considered and the study is done on a particular tower. It is just a small step toward the understanding of the imperfection sensitivity of wind turbine towers under the application of bending moment. Future work will incorporate other types of imperfections and other critical phenomena.

References

ABAQUS (2016), User's Manual: 6.14, Dassault Systems.

Deml, M., Wunderlich, W. (1997). "Direct evaluation of the 'worst' imperfection shape in shell buckling." *Computer Methods in Applied Mechanics and Engineering,* 149 201-222.

Guo, L., Yang, S., Jiao, H. (2013). "Behavior of thin-walled circular hollow section tubes subjected to bending." *Thin-Walled Structures,* 73 281-289.

Jay, A., Myers, A., Torabian, S., Mahmoud, A., Smith, E., Schafer, B. W. (2016). "Spirally welded steel wind towers: Buckling experiments, analysis and research needs." *Journal of Constructional Steel Research,* 125 218-226.

Hutchinson, J.W. (1965). "Axial buckling of pressurized imperfect cylindrical shells." *AIAA Journal,* 3 1461-1465.

Hutchinson, J.W. (2010). "Knockdown factor for buckling of cylindrical and spherical shells subject to reduced biaxial membrane stress." *International Journal of Solid and Structures,* 47 1443-1448.

Karamanos, S. A., Tassoulas, J.L. (1991). "Stability of Inelastic Tubes under External Pressure and Bending." *Journal of Engineering Mechanics,* 117 2845-2861.

Khatri, D. (2010). "Economics of Taller Wind Towers." *Renewable Energy World.*

Koiter, W. T. (1945). "On the stability of elastic equilibrium." *Thesis Deft, H.J. Paris, Amsterdam.*

Kyriakides, S., Shaw, P.K. (1982). "Response and stability of elastoplastic circular pipes under combined bending and external pressure." *International journal of solids and structures,* 18 957-973.

Lindgaard, E., Lund, E., Rasmussen, K. (2010). "Nonlinear buckling optimization of composite structures considering "Worst" shape imperfection." *International Journal of Solids and Structures,* 47 3186-3202.

Mahmoud, A., Torabian, S., Jay, A., Myers, A., Smith, E., Schafer, B. W. (2015). "Modeling protocols for elastic buckling and collapse analysis of spirally welded circular hollow thin-walled sections." *Proceedings of the Annual Stability Conference SSRC'15,* Nashville, Tennessee.

NASA SP-8007 (1965). "Buckling of thin-walled circular cylinders."

Schneider, W., Timmel, I., Hohn, K. (2005). "The conception of quasi-collapse-affine imperfections: A new approach to unfavorable imperfections of thin-walled shell structures." *Thin-Walled Structures,* 43 1202-1224.

Wunderlich, W., Albertin, U. (2000). "Analysis and load carrying behavior of imperfection sensitive shells." *International Journal For Numerical Methods In Engineering,* 47 255-273.